GEOPHYSICS, VOL. 82, NO. 3 (MAY-JUNE 2017); P. KS27–KS39, 16 FIGS., 1 TABLE.
10.1190/GEO2016-0158.1

Simultaneous inversion of multiple microseismic data for event locations and velocity model with Bayesian inference

Zhishuai Zhang[1], James W. Rector[1], and Michael J. Nava[1]

ABSTRACT

We have applied Bayesian inference for simultaneous inversion of multiple microseismic data to obtain event locations along with the subsurface velocity model. The traditional method of using a predetermined velocity model for event location may be subject to large uncertainties, particularly if the prior velocity model is poor. Our study indicated that microseismic data can help to construct the velocity model, which is usually a major source of uncertainty in microseismic event locations. The simultaneous inversion eliminates the requirement for an accurate predetermined velocity model in microseismic event location estimation. We estimate the posterior probability density of the velocity model and microseismic event locations with the maximum a posteriori estimation, and the posterior covariance approximation under the Gaussian assumption. This provides an efficient and effective way to quantify the uncertainty of the microseismic location estimation and capture the correlation between the velocity model and microseismic event locations. We have developed successful applications on both synthetic examples and real data from the Newberry enhanced geothermal system. Comparisons with location results based on a traditional predetermined velocity model method demonstrated that we can construct a reliable effective velocity model using only microseismic data and determine microseismic event locations without prior knowledge of the velocity model.

INTRODUCTION

Human activities, such as hydraulic fracturing, wastewater disposal, enhanced geothermal system (EGS) stimulation, and carbon sequestration, have been shown to induce small earthquakes. Microseismic analysis is the characterization of these small earthquakes for the purpose of monitoring subsurface human activities. The processing of microseismic data involves event location and, in some ideal circumstances, moment magnitude estimation and advanced source parameter and frequency analysis (Eisner and Le Calvez, 2007; Maxwell, 2014). Event location is the basis of almost all other advanced processing. It is a routine, yet in many circumstances, poorly understood, processing procedure in the microseismic industry. Existing methods for microseismic event location include least-squares traveltime inversion (Aki and Richards, 1980; Rutledge and Phillips, 2003), double-difference (Waldhauser and Ellsworth, 2000), coherence scanning (Drew et al., 2005; Duncan Peter and Eisner, 2010), time-reverse imaging (Artman et al., 2010, Artman and Witten, 2011), and even full-waveform inversion (Song and Toksöz, 2011). Due to the often poor signal-to-noise ratio (S/N) of microseismic data, lack of information on velocity models, and limited spatial coverage of monitoring stations, microseismic location uncertainty can be significant (Eisner et al., 2009; Maxwell, 2009). Engineers without in-depth knowledge of microseismic processing might be confounded by the large uncertainty in event location (Hayles et al., 2011). As such, it is crucial to obtain a quantitative understanding of microseismic event location uncertainty before drawing any further conclusions on microseismic data. To improve acceptance of microseismic monitoring, geophysicists must address the following questions: (1) how to improve the absolute accuracy and relative precision of microseismic event location and (2) how to quantify the uncertainty associated with microseismic location estimation.

In microseismic processing, the velocity model is usually the most important factor in determining the accuracy and precision of microseismic event locations (Maxwell, 2009; Warpinski et al., 2009; Gesret et al., 2015). People typically obtain velocity information independently from microseismic data, such as from sonic logs, active-source surveys, or subsurface calibration/perforation shots. Depending on the availability of subsurface information, we can build a velocity model with various complexities such as hetero-

Manuscript received by the Editor 27 March 2016; revised manuscript received 15 November 2016; published online 15 March 2017.
[1]University of California, Berkeley, Department of Civil and Environmental Engineering, Berkeley, California, USA. E-mail: zhishuaizhang@gmail.com; jwrector@lbl.gov; navamj@berkeley.edu.

geneity and anisotropy (Grechka and Duchkov, 2011; Grechka et al., 2011; Grechka and Yaskevich, 2013; Li et al., 2014) for microseismic processing. Moreover, rock properties may change during the treatment process, which requires a time-dependent subsurface velocity model (Tan et al., 2014). In a realistic survey, it can be challenging to build even a 1D velocity model. However, given the abundance of microseismic events in a normal survey, they are a good source of information to calibrate or even construct a velocity model for microseismic location estimation (Douglas, 1967).

Due to the importance of obtaining accurate velocity models in microseismic event location estimation, various studies have been carried out on simultaneous inversion for event locations and the velocity model (Zhang and Thurber, 2003, 2006; Jansky et al., 2010; Grechka et al., 2011; Li et al., 2013, 2014). Jansky et al. (2010) study the feasibility of inverting for a 1D velocity model in various downhole monitoring geometries. Zhang and Thurber (2003, 2006) develop a double-difference tomography method to improve velocity estimations with absolute and relative arrival times. It takes the absolute and relative arrival times into consideration and is successful on microseismic data (Zhang et al., 2009; Zhou et al., 2010). Li et al. (2013, 2014) estimate the Thomsen's parameters from microseismic data by assuming a vertical transverse isotropic model. Grechka et al. (2011) invert for the important anisotropic parameters by assuming a homogeneous velocity model in a downhole microseismic survey. These methods usually apply the traditional least-squares criterion for their inversions. In addition, they usually require determinations of weighting or regularization parameters, which can be challenging to estimate (Monteiller et al., 2005). Just as is typical with most inverse problems, the result can be highly dependent on the processor's subjectivity.

Bayesian inference is a widely used algorithm in subsurface inverse problems (Oliver et al., 2008; Zhang et al., 2014). Tarantola and Valette (1982) and Tarantola (2005) provide a general interpretation of Bayesian inference as a combination of states of information. They derive the statistical framework to combine prior information on model parameters, knowledge of the physical model, and information from observations into a joint probability density. Bayesian inference provides a good solution to earthquake (Monteiller et al., 2005; Myers et al., 2007, 2009) and microseismic event location problems (Poliannikov et al., 2013, 2014; Templeton et al., 2014; Zhang et al., 2015a, 2015b). Due to the fact that parameters are treated as a joint probability density, it has been very successful in model parameter estimation and uncertainty analysis. Compared with traditional methods of quantifying uncertainty (Eisner et al., 2009; Maxwell, 2009), Bayesian inference provides a more comprehensive way to take various sources of information into consideration. In addition, the application of Bayesian inference eliminates the necessity of various weighting parameters that are commonly required by a simultaneous inversion algorithm. Instead, it uses physically understandable parameters to describe the probability distribution of various parameters.

In this paper, we apply Bayesian inference for simultaneous velocity inversion and event location using multiple microseismic event data. Tarantola's (2005) interpretation of Bayesian inference provides the robustness of combining various sources of information in a statistical way. Thus, it makes uncertainty quantification in microseismic event location a straightforward process. With the help of simultaneous inversion, we can estimate effective velocity models for microseismic event locations using only microseismic data. This minimizes the efforts and expense required for a velocity survey. Successful applications of the developed method to synthetic and real microseismic surveys demonstrate its effectiveness. Furthermore, sensitivity analysis provides information on the source of event location uncertainty. As such, the result shows that we can successfully construct a velocity model using microseismic data and obtain reliable event locations without prior information on the velocity model.

In this paper, we first give a brief overview of Bayesian inference and approximate its solution with maximum a posteriori (MAP) estimation and covariance matrix under a Gaussian assumption. Then, we present the algorithm for implementing Bayesian inference for the simultaneous inversion problem. We test the method with a synthetic model and a real microseismic data set from the Newberry EGS site. Finally, we conclude with the discussion of the limitation of our work and potential future directions.

METHODS

In this section, we present the formulation and solution of simultaneous inversion as a Bayesian inference problem. Here, the central idea is to represent all the information we have (forward model, observation, and prior information) with probability densities. Then, using inverse theory, we infer the posterior probability density of the model parameters we would like to know. We define observations as the information we have from a survey and would like to use to improve knowledge of model parameters. Likewise, prior information is defined as what we know about model parameters from knowledge other than the studied survey. Finally, the forward model serves as the link between model parameters (the information we want to know) and observations (the information we have from a survey).

Inverse problem theory

We can denote the model parameters and observable parameters (data) of a physical system as $\mathbf{m}$ and $\mathbf{d}$, respectively. The inverse problem theory (Tarantola, 2005) gives the joint posterior probability density:

$$\sigma(\mathbf{d},\mathbf{m}) = k\frac{\rho_{\mathrm{D}}(\mathbf{d})\rho_{\mathrm{M}}(\mathbf{m})\theta(\mathbf{d}|\mathbf{m})}{\mu_{\mathrm{D}}(\mathbf{d})}, \tag{1}$$

where $\rho_{\mathrm{D}}(\mathbf{d})$ is the probability density in data space representing the information given by a measurement, $\rho_{\mathrm{M}}(\mathbf{m})$ is the prior information on model parameters, $\theta(\mathbf{d}|\mathbf{m})$ is the conditional probability density of data $\mathbf{d}$ given model parameters $\mathbf{m}$, and $\mu_{\mathrm{D}}(\mathbf{d})$ is a homogeneous probability density in the data space.

The marginal probability density of model parameters $\mathbf{m}$ is the integration of the joint probability density over the entire data space $\mathfrak{D}$:

$$\sigma_{\mathrm{M}}(\mathbf{m}) = \int_{\mathfrak{D}} d\mathbf{d}\sigma(\mathbf{d},\mathbf{m}). \tag{2}$$

If the model and data space of the system are linear, under a Gaussian probability density assumption, the posterior probability density of the model parameters can be expressed by

$$\sigma_M(\mathbf{m}) = c\ \exp\left\{-\frac{1}{2}[\mathbf{g}(\mathbf{m}) - \mathbf{d}_{obs}]^T\mathbf{C}_D^{-1}[\mathbf{g}(\mathbf{m}) - \mathbf{d}_{obs}] - \frac{1}{2}(\mathbf{m} - \mathbf{m}_{prior})^T\mathbf{C}_M^{-1}(\mathbf{m} - \mathbf{m}_{prior})\right\}, \quad (3)$$

where $\mathbf{g}(\cdot)$ is the forward operator for the prediction of observable parameters from model parameters $\mathbf{m}$ and $\mathbf{m}_{prior}$ is the prior information on the model parameters. The covariance matrix $\mathbf{C}_D$ is the addition of observation uncertainty covariance matrix $\mathbf{C}_d$ and theoretical uncertainty covariance matrix $\mathbf{C}_T$. Here, $\mathbf{C}_M$ is the covariance matrix of the prior information and c is a normalization constant. A derivation and detailed discussion of equation 3 is presented by Tarantola (2005).

Maximum a posteriori estimation

Even if all the information we have are of the Gaussian type, as a result of the nonlinear operator $\mathbf{g}(\cdot)$, the posterior probability density may take a more complex non-Gaussian form (Oliver et al., 1996) that, in general, is difficult to be predicted. Two general approaches are considered in the literature for characterizing the resulting posterior probability density. The first approach aims to estimate statistics of the posterior probability density, such as its mean and covariance, which provide incomplete, yet important, characterization of the conditional parameter distribution. The second approach focuses on approximating the posterior probability density by generating many conditional realizations that enable a systematic approach to uncertainty quantification, such as Markov chain Monte Carlo (MCMC). In this study, we use the maximum a posteriori estimation and its posterior covariance approximation under a Gaussian assumption, which lies in the first category, to characterize the model parameters.

The MAP estimation aims at finding the mode of the posterior probability density $\sigma_M(\mathbf{m})$:

$$\mathbf{m}_{MAP} = \arg\max_{\mathbf{m}} \sigma_M(\mathbf{m}). \quad (4)$$

Or equivalently minimizes

$$O(\mathbf{m}) = \frac{1}{2}[\mathbf{g}(\mathbf{m}) - \mathbf{d}_{obs}]^T\mathbf{C}_D^{-1}[\mathbf{g}(\mathbf{m}) - \mathbf{d}_{obs}] + \frac{1}{2}(\mathbf{m} - \mathbf{m}_{prior})^T\mathbf{C}_M^{-1}(\mathbf{m} - \mathbf{m}_{prior}). \quad (5)$$

The above minimization can be implemented using a Gauss-Newton method (Oliver et al., 2008; Li and Jafarpour, 2010). By taking the derivative of the objective function with respect to $\mathbf{m}$ and rearranging, we obtain

$$\mathbf{m}^{n+1} = [(\mathbf{C}_M^{-1} + \mathbf{C}_M^{-1T}) + \mathbf{G}^{nT}(\mathbf{C}_D^{-1} + \mathbf{C}_D^{-1T})\mathbf{G}^n]^{-1} \times \{(\mathbf{C}_M^{-1} + \mathbf{C}_M^{-1T})\mathbf{m}_{prior} + \mathbf{G}^{nT}(\mathbf{C}_D^{-1} + \mathbf{C}_D^{-1T}) \times [\mathbf{d}_{obs} - \mathbf{g}(\mathbf{m}^n) + \mathbf{G}^n\mathbf{m}^n]\}, \quad (6)$$

where $\mathbf{G}$ is the sensitivity matrix with elements $G_{ij} = \partial g_i/\partial m_j$. Once the MAP estimate $\mathbf{m}_{MAP}$ is found, the posterior covariance matrix $\mathbf{C}_{m,MAP}$ can be approximated through linearization about the MAP estimate (Tarantola, 2005) as

$$\mathbf{C}_{m,MAP} = \mathbf{C}_M - \mathbf{C}_M\mathbf{G}_{MAP}^T(\mathbf{G}_{MAP}\mathbf{C}_M\mathbf{G}_{MAP}^T + \mathbf{C}_D)^{-1}\mathbf{G}_{MAP}\mathbf{C}_M. \quad (7)$$

Or equivalently,

$$\mathbf{C}_{m,MAP} = (\mathbf{G}_{MAP}^T\mathbf{C}_D^{-1}\mathbf{G}_{MAP} + \mathbf{C}_M^{-1})^{-1}. \quad (8)$$

Equation 7 is more computationally efficient for high-dimensional models.

Simultaneous inversion for event locations and velocity model

The implementation of the inversion method developed above in the simultaneous estimation of event locations and the velocity model includes the definition of model parameters, prior information on model parameters, measurement, and the forward model.

Ideally, the model should include all the uncertainty parameters that have large impacts on the prediction of the observable parameters. On the other hand, a model space with too large a dimension may cause the inverse problem to be ill-posed. The velocity model we use in this study is a two-layer model with a constant velocity gradient for each layer. The velocity model parameters to be estimated include the P-wave velocity at a reference elevation, P-wave velocity gradient for each of the two layers, the elevation of the two-layer interface, and V_P/V_S. Specifically, for a system with N microseismic events, the model parameter $\mathbf{m}$ is a vector of length $4N + 5$, including the space and time coordinate $[x, y, z, t_o]^T$ for each event and the five parameters for velocity model characterization.

Normally, we have very limited prior information on microseismic event locations and occurrence times before inversion. Therefore, we can use any reasonable locations along with a relatively large uncertainty to approximate a homogeneous probability density. For prior information on the velocity model, we can use prior information from other independent geophysical surveys with its corresponding uncertainty. Alternatively, we can even use a homogeneous probability density because we can parameterize the earth model with a minimum number of essential parameters so that the model can be determined purely using the microseismic events' arrival-time information.

Measurements include any available P- and/or S-wave arrival times for each event at each station. Because the observations of arrival times at various stations for these events are made individually, we will assume that there is no correlation between various observations, and thus covariance matrix $\mathbf{C}_d$ becomes a diagonal matrix with variance at corresponding diagonal positions. The determination of theoretical uncertainty covariance matrix $\mathbf{C}_T$ requires specific analysis of the model itself. We will give a preliminary analysis of this with a synthetic example in the next section.

The forward model calculates the arrival time from the microseismic event location to a receiver location. The raypaths in a constant gradient model can be obtained analytically (Slawinski and Slawinski, 1999). We solve the two-layer problem semianalytically by iterating for the ray parameter that is common to the seismic rays in both layers.

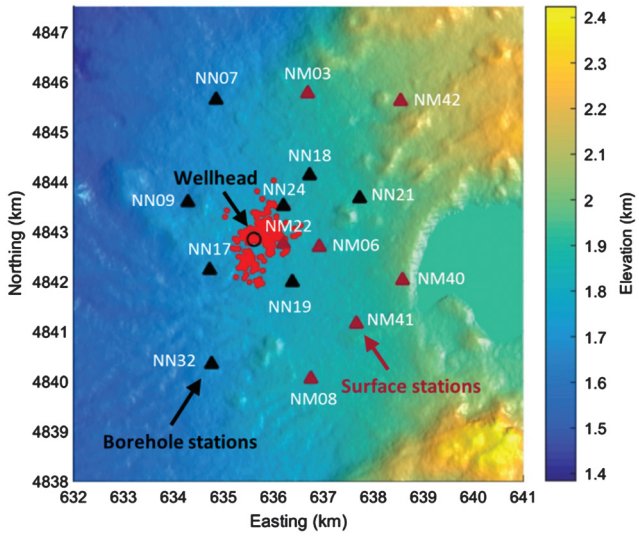

Figure 1. Map of surface stations and shallow borehole stations for microseismic monitoring. Surface stations provide complementary azimuthal coverage to the shallow borehole stations. The red dots indicate the locations of microseismic events.

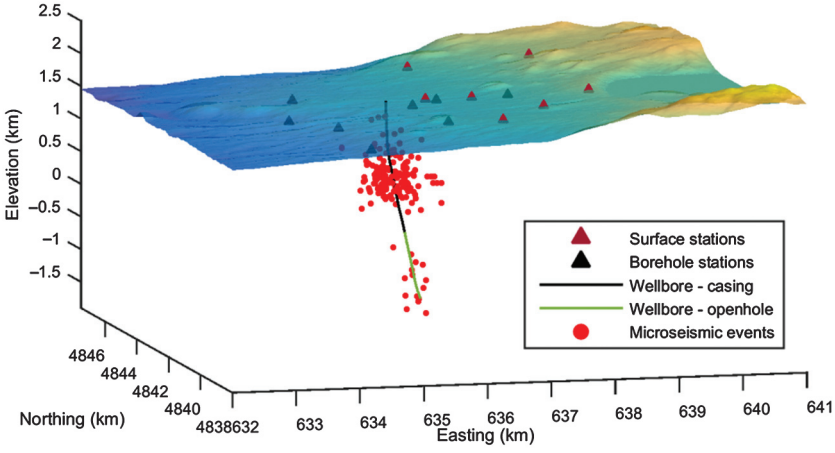

Figure 2. Relative location of the seismic stations, well path, the open-hole portion of the well, and recorded microseismic events. The seismic stations provide good azimuthal coverage above the designed stimulation zone.

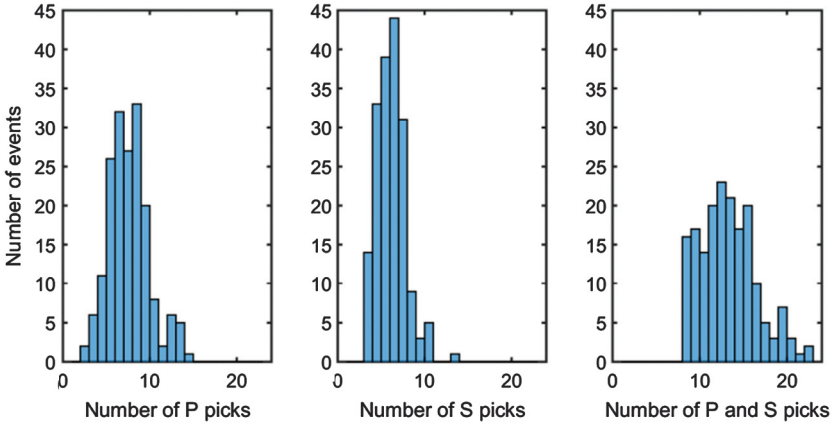

Figure 3. Histogram of the number of available picks for real data as well as for synthetic study. For stability purposes, we only studied the 179 events with at least eight picks available.

MICROSEISMIC SURVEY IN NEWBERRY EGS SYSTEM

We applied the developed simultaneous inversion algorithm to synthetic and real data from the Newberry EGS demonstration site (Petty et al., 2013). Fluid injection for hydroshearing (Petty et al., 2013) has induced microseismic events in this area. A contractor conducted an active-source seismic survey to determine a 1D velocity model for microseismic event location. Event locations were estimated by the contractor using picked P- and S-wave arrival times. With the same picked arrival times, we relocated the microseismic events using our simultaneous inversion approach. The analysis of the inversion result shows that the simultaneous inversion is able to construct an effective velocity model by matching the observed arrival times of microseismic events. It also demonstrates the robustness of our algorithm over the traditional location method, which requires a predetermined velocity model.

Newberry EGS demonstration

The EGS system under study is located at the Newberry volcano in Central Oregon. According to the stimulation plan (Osborn et al., 2010, 2011; Petty et al., 2013), an existing well, NGC 55-29, was stimulated with a hydroshearing technique due to the high temperature and lack of permeability of the nearby formation. Well NGC 55-29 has a total depth of 3066 m with an open hole from 1790 m to its total depth. In contrast to well-known hydraulic fracturing, the hydroshearing technique used in this demonstration stimulated the formation below its minimum principal stress. The stimulation induced shear failures of preexisting natural fractures in the target formation. This process was monitored with seismometers on the surface and in shallow boreholes. After the completion of the stimulation, two production wells will be drilled based on microseismicity clouds generated during stimulation of the injection well, NGC 55-29. These three wells will form a circulation system for long-term testing and performance assessment.

Microseismic survey

The survey was conducted with 15 seismic stations, which include seven seismometers placed on the surface and eight placed in shallow boreholes as shown in Figure 1. A permitting issue led to poor azimuthal coverage of the shallow borehole stations. However, surface stations provide complementary coverage. Eight shallow monitoring holes were drilled to depths between 213 and 246 m. A primary objective is to reach below the water table and the highly attenuating cinders and debris flows (Cladouhos et al., 2013). The stimulation of NGC 55–29 began on 17 October 2012 and went until 7 December 2012, and the first detected microseismic event occurred on 29 October. A total of 204 events with reasonably high S/Ns were recorded until 31 December 2012. Figure 2 provides

a 3D view of the relative location of the seismic stations, the well path, the open-hole portion of the well, and the recorded microseismic events.

To process the microseismic data set, the contractor has picked P- and/or S-wave arrival times for all event-station pairs whenever possible. To ensure the stability of the inversion, we only used events with at least eight picks available, which leaves 179 out of 204 events to meet this criterion. The histogram of the number of available picks for these 179 events is shown in Figure 3. The contractor also derived a 1D velocity model by conducting a dedicated active-source seismic survey. With the obtained velocity model, they located the microseismic events by minimizing the misfit between the observed and modeled P- and/or S-wave arrival times. A velocity model constructed by Matzel et al. (2014) with interferometry is also used for comparison.

SYNTHETIC EXAMPLE

First, we studied a synthetic model with the same acquisition geometry as the field survey. The histograms of the number of available picks for all the 179 events are the same as the field data shown in Figure 3.

Gaussian random error

The first experiment is to study the effect of Gaussian random errors on event locations and velocity model estimation. We assume that the velocity model has the potential to characterize the true model perfectly. That is, the theoretical uncertainty covariance matrix $\mathbf{C}_T$ is zero. To achieve this goal, we use a two-layer velocity model for the synthetic data set construction and the inversion. Five variables can completely characterize this velocity model: the P-wave velocity at a reference elevation (fixed at 1.5 km in this study), velocity gradient of the upper layer, velocity gradient of the lower layer, elevation of the two layer interface, and V_P/V_S. The true values used for forward modeling are in the first column of Table 1. The velocity model represented by these parameters is the red line in Figure 4.

The P- and S-wave traveltimes are calculated semianalytically for each event-station pair, and a Gaussian noise with standard deviation (SD) of 0.022 s is added as a representation of random

Table 1. True, prior, and MAP estimated velocity model parameters and their associated standard deviations that represent uncertainties.

Parameter	True value	Prior mean	Prior SD	MAP value	Posterior SD
Reference elevation (km)			1.50 (fixed)		
Reference velocity (km/s)	2.46	2.00	1.00	2.47	0.03
Upper gradient (1/s)	2.76	1.50	2.00	2.80	0.07
Lower gradient (1/s)	0.74	1.50	2.00	0.78	0.02
Interface elevation (km)	1.07	0.80	0.50	1.10	0.04
V_P/V_S	1.72	1.65	0.25	1.72	0.00

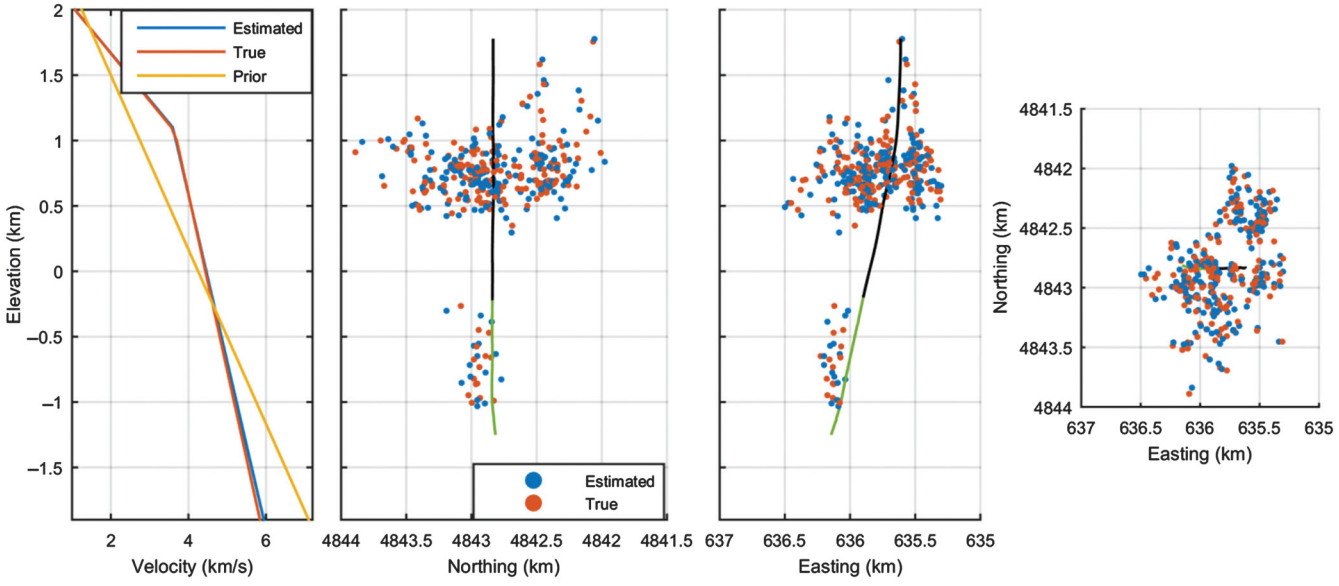

Figure 4. A two-layer velocity model was used for the synthetic study. Compared with the prior velocity model, the estimated model is much closer to the true velocity model. The simultaneous inversion successfully estimated the microseismic event locations. The estimation error in the vertical direction is larger than that in the horizontal direction.

error. We assume that there is little prior information on the microseismic event locations and velocity model parameters. A multivariate normal distribution with reasonable mean and sufficiently large standard deviation can approximate a homogeneous probability density for prior information and the initial model. Prior mean values and standard deviations of the velocity model parameters are listed in columns 2 and 3 of Table 1. The corresponding velocity model is represented by the yellow line in Figure 4.

A comparison between true microseismic locations and the estimated locations is also shown in Figure 4, and the estimated 90% confidence ellipsoids are shown in Figure 5. The size of the error ellipsoids mainly depends on two factors: the number of available picks and the location of an event. The size of the error ellipsoids will decrease as the number of available picks increases. As an event goes deeper, its location uncertainty will become larger. In addition, we observed that the vertical location uncertainty is larger than the horizontal uncertainty, which is commonly known for surface-acquired microseismic data (Eisner et al., 2009). To verify the effectiveness of the MAP estimation and uncertainty approximation, we calculated the error ellipsoids of the estimation from 10% to 90% at a 10% interval. Then, for ellipsoids corresponding to each error value, we counted the ratio of locations estimated within the predicted ellipsoids as the actual estimation confidence. Its relation with the predicted confidence with equation 7 or 8 is shown in Figure 6. The match between these two confidences verifies the effectiveness of the MAP estimation and the uncertainty approximation.

The MAP estimation of velocity model parameters and their uncertainties are also shown in Table 1 and the blue line in Figure 4. We can see from the result that the velocity model can be successfully recovered by simultaneous inversion using multiple microseismic data. The MAP values of the velocity model parameters are much closer to the true values compared with the prior estimates. In addition, the standard deviations of the posterior probability distribution are good representations of the deviations of the MAP values. This verifies the effectiveness of the Bayesian inference for our multiple events location problem.

Velocity model parameterization error

The two-layer velocity model seems oversimplified at first glance. However, our study in this subsection shows that it is possible to characterize a multiple-layer model, which has more parameters that may cause unstable inversion with a two-layer velocity model. In this synthetic example, the velocity model used for data set construction is a multiple-layer model based on Matzel et al.'s (2014) interferometry estimation at the Newberry EGS site (the red line in Figure 7). Because the purpose of this section is to study the velocity parameterization error $\mathbf{C}_T$ introduced by a two-layer velocity model, no picking error was added to the forward modeling result. That is, $\mathbf{C}_d$ is zero. All other parameters stay the same as the previous section.

The result shows that the estimated velocity model (the blue line in Figure 7) captures the multiple-layer model relatively well. In addition, the standard deviation of data misfit is 0.0034 s for the P-wave and 0.0045 s for the S-wave. This parameter is a represen-

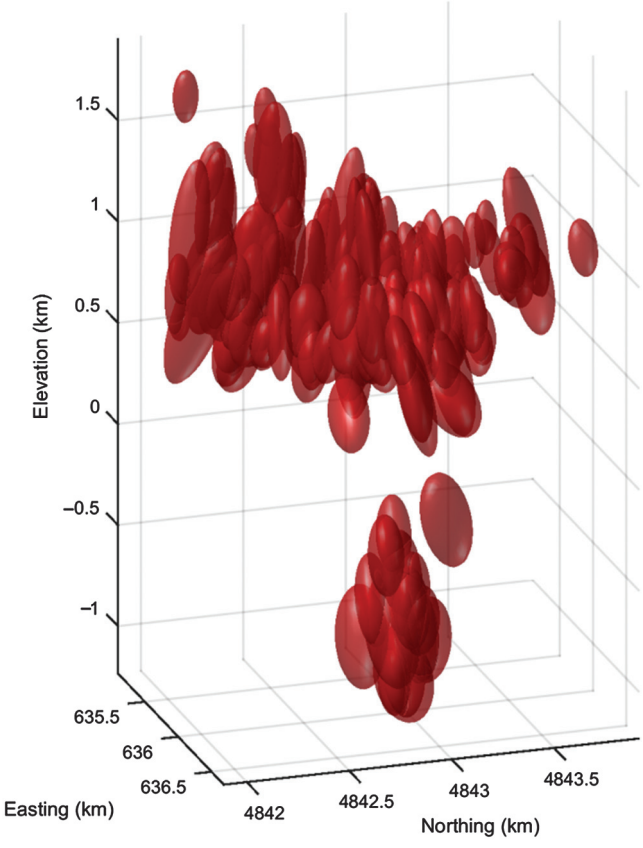

Figure 5. The 90% confidence ellipsoids of the estimation in the synthetic study. The size of the ellipsoid increases as the depth of the event increases or as the number of available picks decreases. The uncertainty in the vertical direction is larger than that in the horizontal direction due to the limitation of the survey geometry.

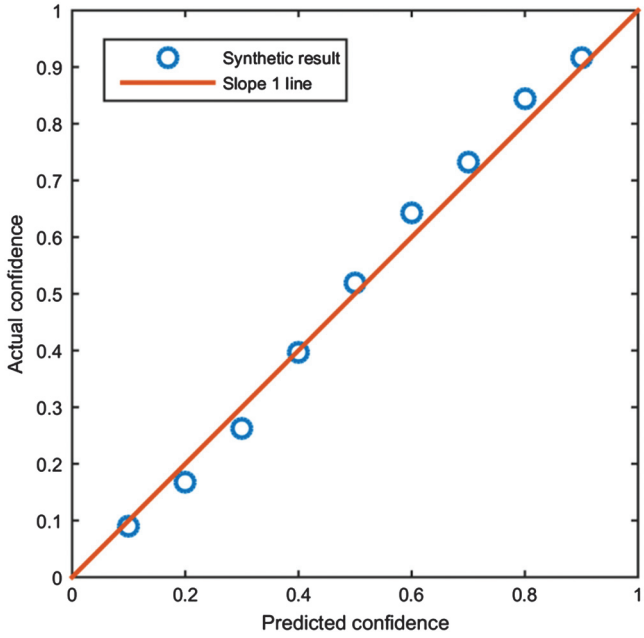

Figure 6. The relationship between the theoretical prediction and the actual prediction confidence for the synthetic study with a Gaussian picking error. The Bayesian inference successfully predicted the location uncertainty of the estimation.

tation of theoretical uncertainty covariance matrix $\mathbf{C}_T$. It is relatively small compared with observation error $\mathbf{C}_d$ in this kind of survey design. As such, it is reasonable to use a two-layer model instead of a multiple-layer model for the simultaneous inversion problem. Additionally, the theoretical uncertainty covariance matrix $\mathbf{C}_T$ introduced by the simplification from a multiple-layer velocity model to a two-layer velocity model is not significant.

Admittedly, the ideal earth model is a 3D model. The parameterization error studied in this section is introduced by the simplification from a multiple-layer 1D model. The actual parameterization error can be larger. Estimating a 3D model with adequate regularization is also possible to reduce parameterization error and deserves further investigation.

FIELD DATA

Finally, we applied the simultaneous inversion algorithm to the field data. Figure 8 shows our location result along with the result processed by the contractor. Both of the results show two event clus-

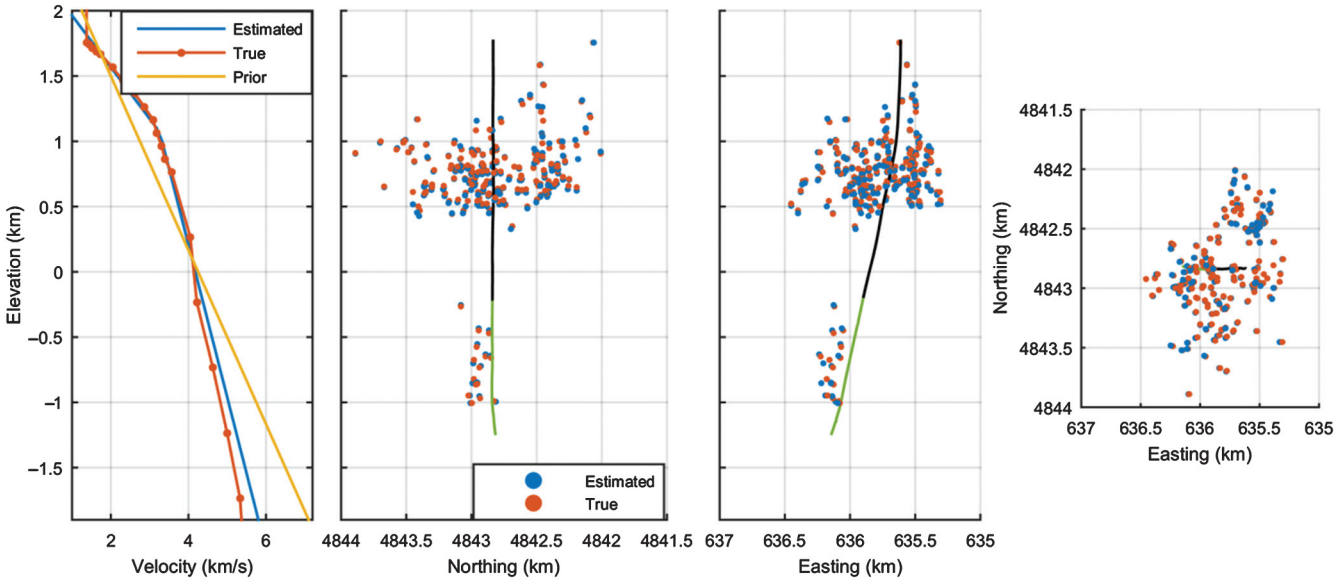

Figure 7. The estimated two-layer velocity model can capture the trend of the true multiple-layer model. It did not introduce significant error to the microseismic event locations. This shows that it is adequate to use a two-layer model in this specific scenario.

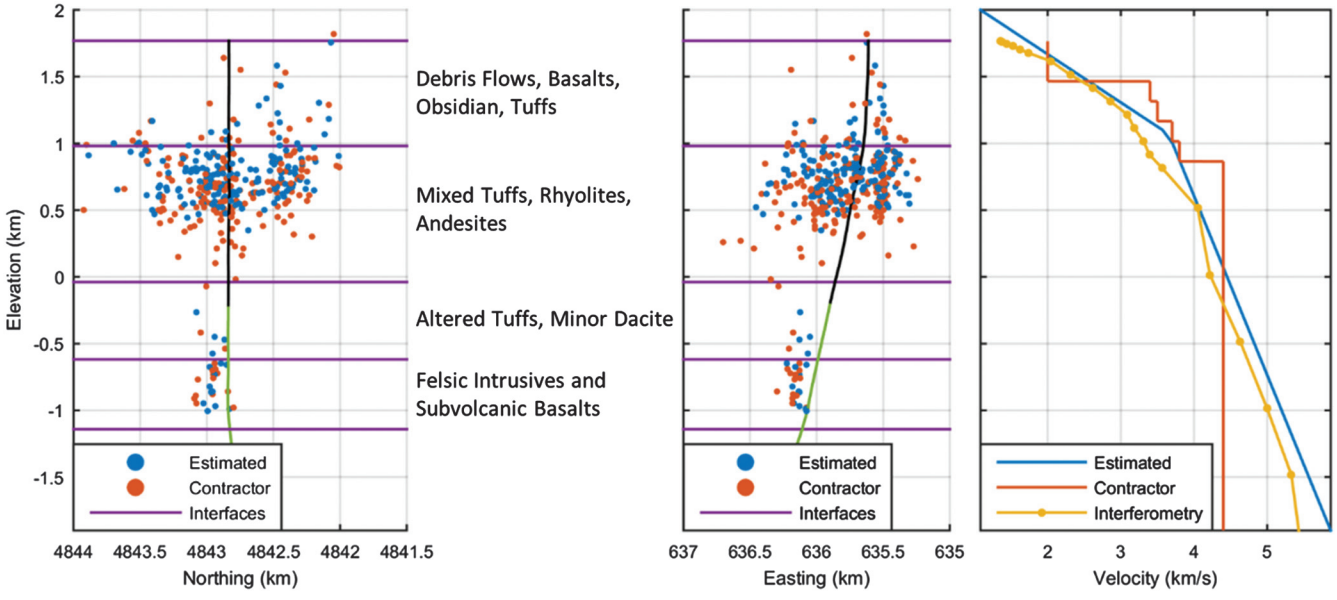

Figure 8. Comparison between our simultaneous location result and that provided by the contractor. The simultaneous location result is more clustered than the contractor's result. There is a significant difference in the lower boundaries of the shallow events for the contractor's result (around the elevation of 0 km) and our simultaneous inversion (around the elevation of 0.5 km) due to the difference in the velocity model. The simultaneously inverted P-wave velocity model is very close to the model obtained by seismic interferometry compared with the contractor's model.

ters: the shallow events above 0 km elevation and the deep events near the open-hole portion of the well. The target zone of the stimulation is the formation at the depth of the open hole. However, we see many more microseismic events in the shallow area. After investigation, a borehole television survey found that it is a result of fluid loss from a cracked casing.

Although these two results share a similar microseismic distribution pattern, we find that the microseismic event locations provided by the contractor (red dots) are more scattered than those estimated by our method (blue dots). Another significant difference is that the lower boundary of the shallow events is around the elevation of 0 km, whereas that of the simultaneous inversion is approximately 0.5 km. The histogram of the differences between these two results

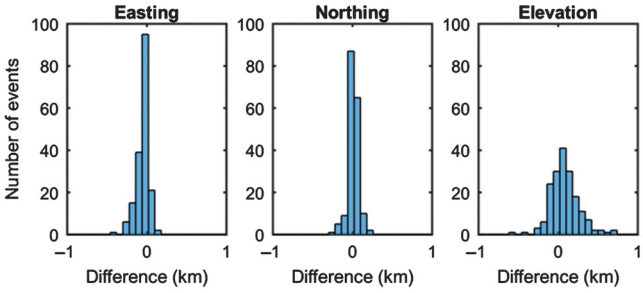

Figure 9. The histogram of differences between the MAP estimated result and that provided by the contractor. The histogram in elevation differences has a broader distribution due to the larger location uncertainty in the vertical direction. The positive mean value of this distribution is mainly a result of the low V_P/V_S used by the contractor.

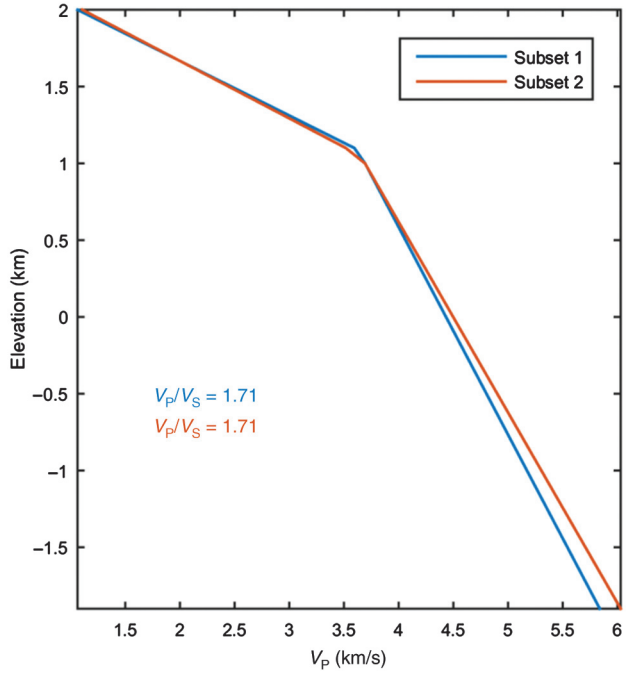

Figure 10. Velocity model estimated with two independent subsets of the data. The similarity between these two models verifies the stability of the simultaneous inversion.

(simultaneous inversion locations − the contractor's locations) is shown in Figure 9. The distribution of the differences in the easting direction has a negative mean value, whereas that in the northing direction has a mean value around zero. This may be a result of the uneven distribution of the surface and borehole stations in the easting direction. Namely, there are more borehole stations to the west of the stimulation zone than to the east. The distribution of the differences in elevation has a much broader distribution due to the large location uncertainty in the vertical direction. The positive mean value of this distribution is mainly a result of the low V_P/V_S used by the contractor compared with our estimated V_P/V_S as will be further discussed in this section.

The right of Figure 8 is the plot of the velocity models used by the contractor, estimated by our simultaneous inversion using microseismic arrival times, and obtained with seismic interferometry by Matzel et al. (2014). The V_P/V_S value used by the contractor is approximately 1.65, whereas we estimated it to be approximately 1.72. From the comparison of V_P values, we find that the velocity model estimated with our method matches the result of the seismic interferometry relatively well. However, the velocity model used by the contractor is higher than these two results at the elevation interval between 0.5 and 1.5 km. Because the contractor estimated the velocity model with an active-source seismic survey, one possible explanation to the difference between the simultaneous inverted model and the contractor's model is that the raypaths in the active seismic survey can be different from the raypaths in the microseismic survey. With the simultaneous inversion, we were able to construct a velocity model consistent with the raypath coverage of the microseismic survey. To further verify the stability of our simultaneous inversion algorithm for velocity estimation, we randomly divided the 179 microseismic events into two subsets, each of which consists of 90 or 89 events. Then, we estimated the velocity model independently with each of these subsets. The velocity model obtained is shown in Figure 10. Although these two velocity models are obtained using two independent microseismic data sets, they match each other very well in terms of V_P values as well as V_P/V_S. This demonstrates the stability of the simultaneous inversion for this data set. We may also build velocity models with nonrandom subsets of microseismic events to study the variance over space or time. We have divided the whole 179 events into an east subset (90 events) and a west subset (89 events), as well as a north subset (90 events) and a south subset (89 events). With these subsets of microseismic events, we carried out simultaneous inversion, and the inverted velocity models are shown in Figure 11. From this comparison, we can see the V_P and V_P/V_S of the deeper layer are larger for the west and south subsets. This may be a result of the fact that the raypath-covered area is dipping down to the southwest direction (Figure 1). Similarly, we may also divide the microseismic events into early and late subsets to study the change of the earth model over time.

Another advantage of the simultaneous inversion with Bayesian inference is its ability to capture the relationship among various model parameters during the inversion (Poliannikov et al., 2013). Figure 12 shows the posterior correlation matrix of the locations and occurrence times of a deep event, a shallow event, and the five velocity parameters. From this covariance matrix, we can see a relatively strong positive correlation between the V_P/V_S and event elevations. This means that an event elevation will increase (decrease in depth) as the V_P/V_S value increases. Thus, the higher V_P/V_S ratio in

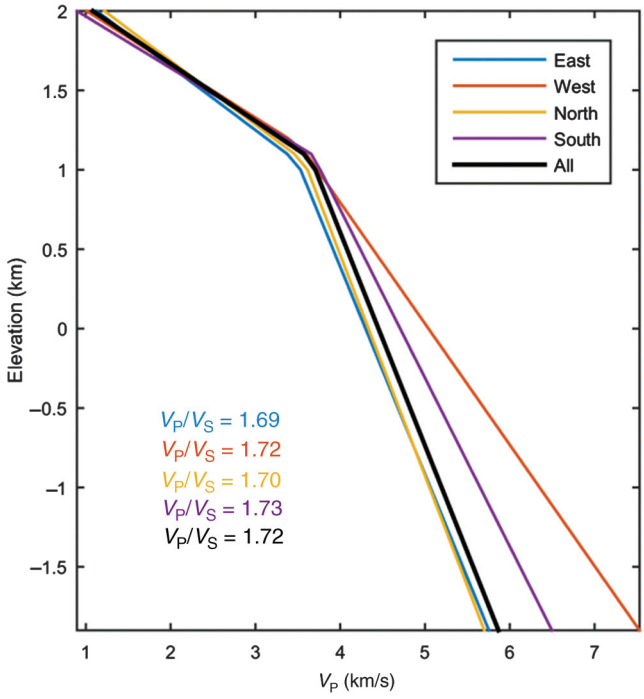

Figure 11. Velocity models estimated with microseismic events in various directions. The V_P and V_P/V_S of the deeper layer are larger for the west and south event subsets. This may be caused by the dipping of the area downward to the southwest direction (Figure 1).

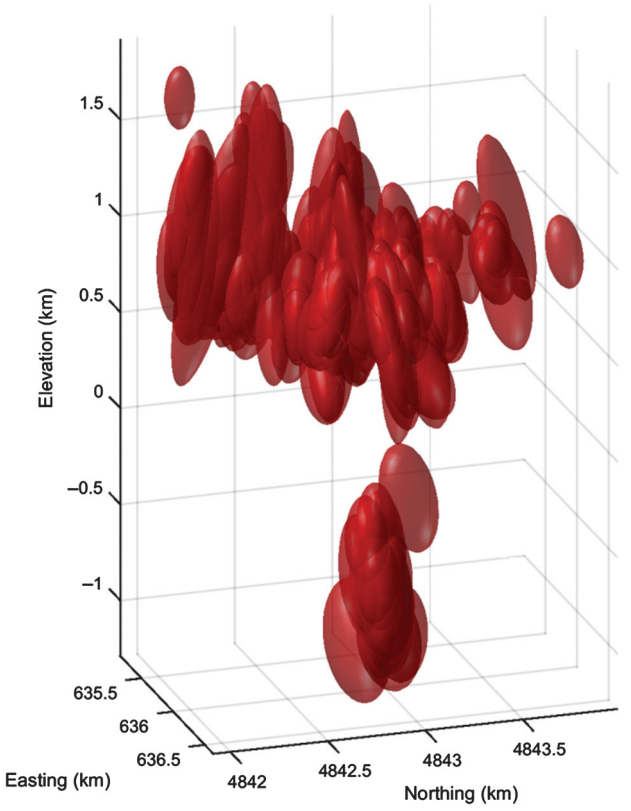

Figure 13. The 90% confidence ellipsoids of the estimation of the field data. It shows a similar pattern with the synthetic case. Because the field data include random picking error and the velocity model parameterization error, the size of the confidence ellipsoids is larger than those in the synthetic case.

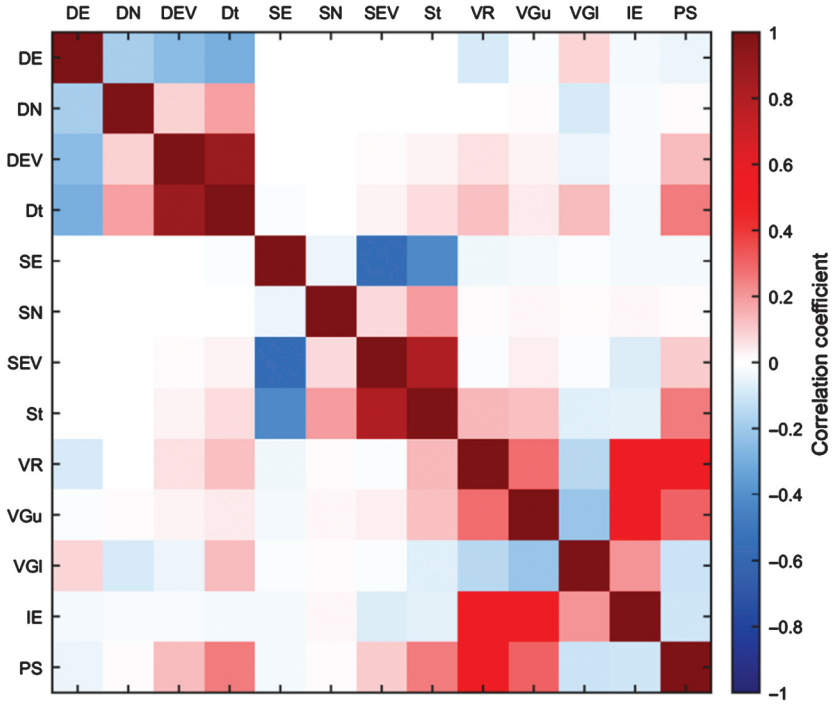

Figure 12. Correlation matrix of a deep event, a shallow event, and five velocity parameters. DE, the easting of the deep event; DN, the northing of the deep event; DEV, the elevation of the deep event; Dt, the occurrence time of the deep event; SE, the easting of the shallow event; SN, the northing of the shallow event; SEV, the elevation of the shallow event; St, the occurrence time of the shallow event; VR, velocity at the reference elevation of 1.5 km; VGu, velocity gradient of the upper layer; VGl, velocity gradient of the lower layer; IE, layer interface elevation; and PS, V_P/V_S.

the simultaneous inversion explains why the inverted elevations are systematically larger than those of the contractor's result.

The 90% confidence ellipsoids of the estimation are shown in Figure 13. The error ellipsoids share a similar shape and pattern with those from the synthetic case in Figure 5. However, they are larger because the field data includes both random picking error and the velocity model parameterization error.

An example of the improvement in the arrival time match is shown in Figure 14. It is a typical event that occurred at the elevation of 0.66 km. The geophone stations are sorted according to the arrival times of the event. Thanks to the simultaneous inversion, the match between the observation and the theoretical prediction has been improved. However, we did not see a systematic change in the arrival-time moveout. This may be due to the irregular geometry of the acquisition or uncertainties resulting from sources other than the velocity model, such as statics.

Figure 15 shows the located microseismic events color coded by their occurrence times. From the map view of these events, it is apparent that the early events are mostly near the well, and the late events spread over the entire area. This is because of the time necessary for the propagation of the stimulation fluid to the field far away from the stimulation well.

Templeton et al. (2014) compared the well head pressure, flow rate information, and the histogram of the microseismic events as shown in Figure 16. There is a good correlation between the well head pressure and the number of microseismic events. The events we are mostly interested in are the small clustered events around the open-hole portion of the well because they are at the target zone. The black dots in Figure 16 show the occurrence times of these deep events. Apparently, they are strongly correlated with the well head pressure. Microseismic events in the target zone only occur when the well head pressure is above approximately 1500 psi due to the fluid loss at the crack as mentioned previously.

DISCUSSION

The MAP point and the covariance matrix approximation of the posterior PDF under a Gaussian assumption are efficient but have some limitations. For example, they may encounter a local minimum problem in the optimization process. The non-Gaussian information and nonlinearity of the problem may also result in a significant bias of this estimation. In these cases, a more sophisticated solution, such as MCMC to the posterior probability density, should be used.

Double-difference earthquake location shows that theoretical error can be significantly reduced by using traveltime differences between nearby events as observations. This correlation between nearby events can be reflected in the off-diagonal entries of the theoretical uncertainty covariance matrix $\mathbf{C}_T$. This may be a more efficient method compared with the double-difference location or double-difference tomography due to its low-dimensional data space. Further study will be necessary to make full use of Bayesian inference.

The parameterization of the velocity model can also be a challenging task. It is a trade-off between the accuracy of a model and the well-posedness of the inverse problem. Parameters sensitive to the observations should be chosen, and those insensitive to the

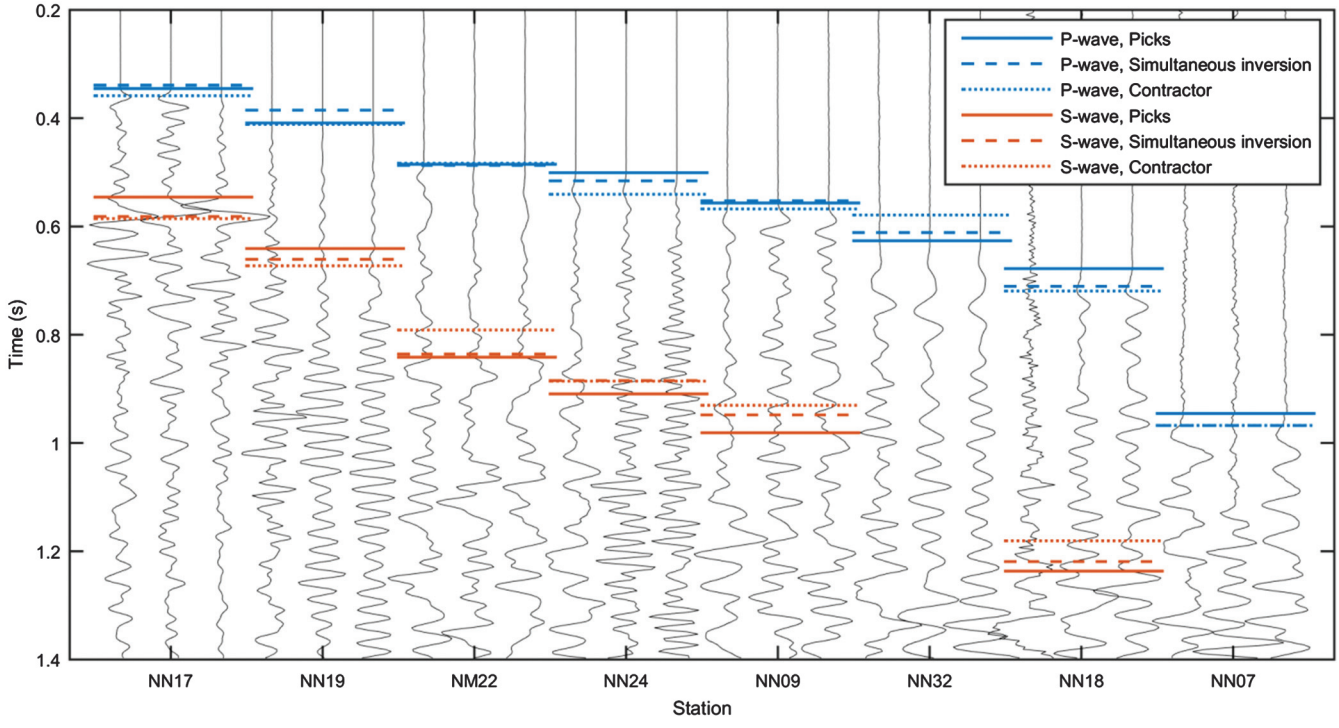

Figure 14. Comparison between picks, arrival times predicted by the contractor's model, and arrival times predicted by simultaneous inversion. Simultaneous inversion was able to improve the match between the theoretical prediction and the real data. However, the improvement is not significant and we did not see a systematic change in the arrival time moveout, probability due to uncertainties resulting from sources other than the velocity model, such as statics.

observations should be avoided if possible. With careful parameterization of the velocity model and a proper prior constraint on the model, tomography using microseismic data might be promising. Grechka and Duchkov (2011) and Grechka et al. (2011) use singular value decomposition to study the roles various anisotropy parameters play in microseismic inversion. They also study the traveltime fit that one can achieve with various numbers of the most important parameters. A similar process can be used to aid in the parameterization of the velocity model in specific acquisition geometries.

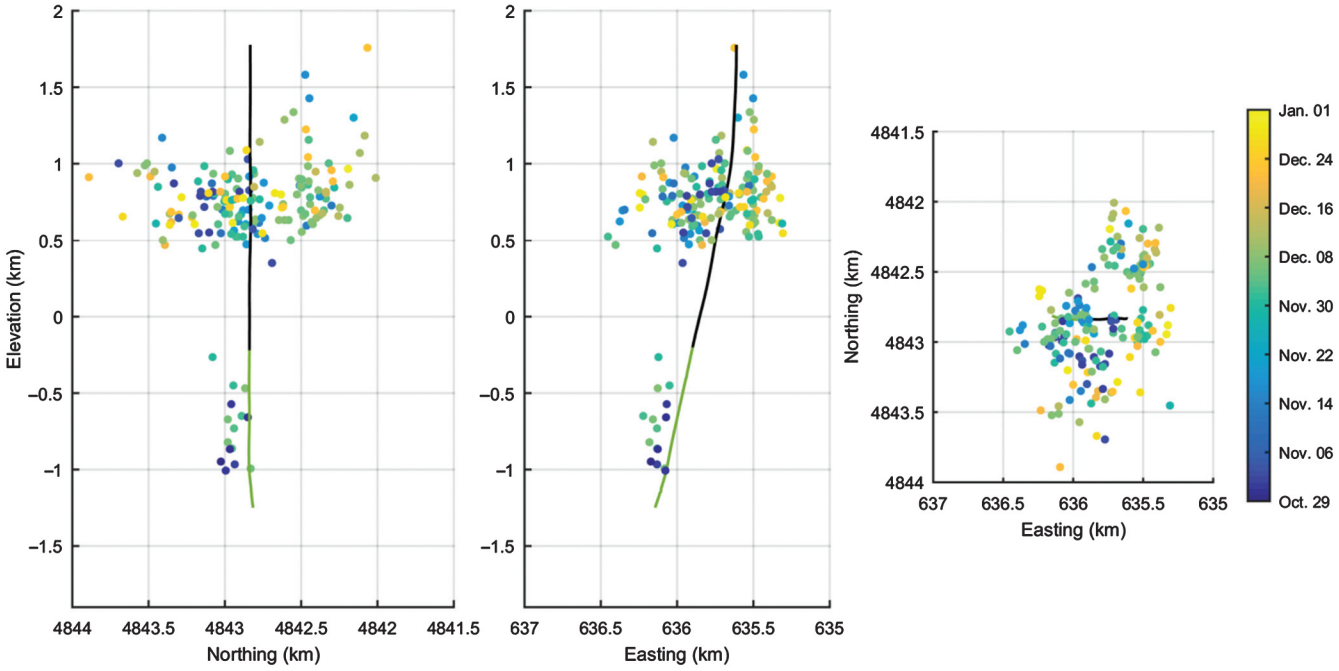

Figure 15. Microseismic events color coded by their occurrence times. Early events only occur near the stimulation well. Late events can be either close to or far away from the stimulation well.

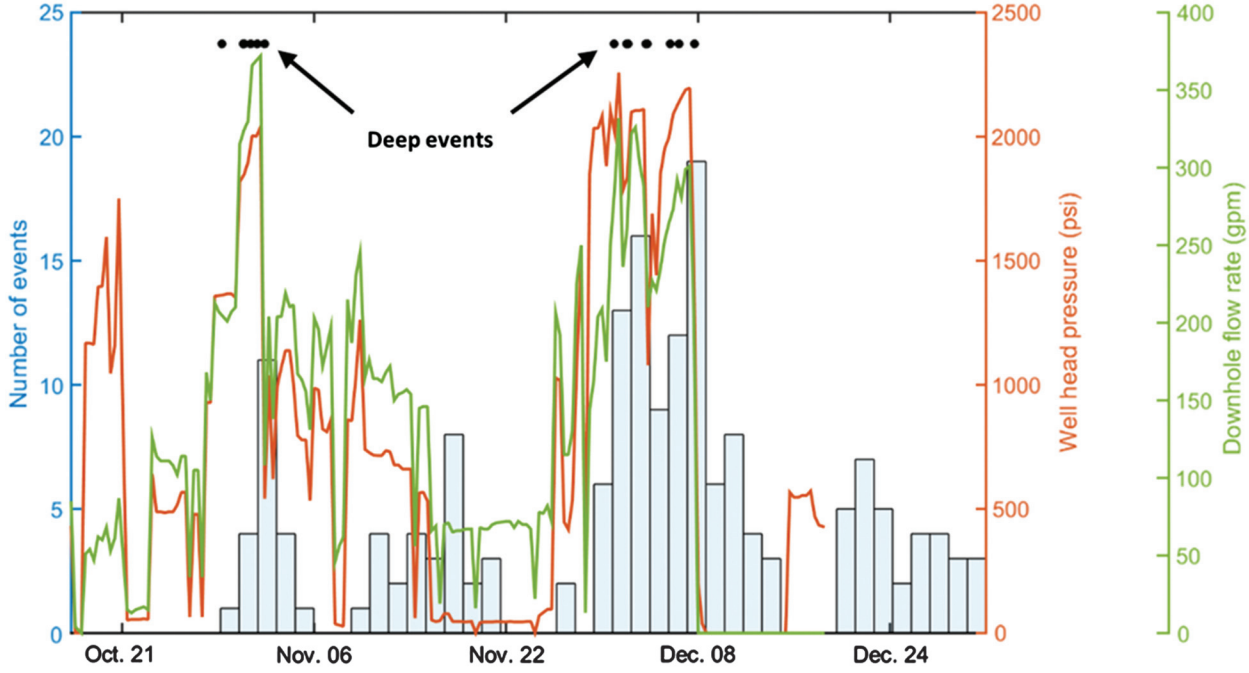

Figure 16. Well head pressure, flow rate information, and the histogram (blue bins) of microseismic events. Microseismic events in the target zone only occur when the well head pressure is above approximately 1500 psi.

If the prior knowledge of the earth model is poor, then the number of microseismic events should be sufficient to constrain the earth model. This makes the application of the simultaneous inversion challenging for the initial state of the hydraulic stimulation. For cases with a relatively good prior earth model, the Kalman filter might be a promising tool to integrate information during the continuous stimulation process (Kalman, 1960).

CONCLUSION

We built the framework for simultaneous inversion of multiple microseismic data for event location and velocity model parameter estimation with Bayesian inference. MAP estimation and the covariance matrix under the Gaussian assumption give an efficient and reasonable approximation to the posterior probability distribution. In addition, Bayesian inference enables the uncertainty to be quantified. The application of the developed location algorithm on a synthetic example and the Newberry EGS data shows that we can successfully construct a velocity model from microseismic data as well as estimate the microseismic event locations. The synthetic study shows that the location uncertainty is typically large in the vertical direction due to the limitation of the acquisition geometry, and the situation is worse as the event goes deeper. Implementation on real microseismic data from the Newberry EGS system shows the possibility of constructing a velocity model purely from microseismic data. With the effective velocity model conforming to the microseismic data, we were able to estimate the microseismic event locations without prior knowledge of the earth model.

ACKNOWLEDGMENTS

We would like to acknowledge S. C. Myers, G. Johannesson, and W. Hanley at the Lawrence Livermore National Laboratory for their inspiring work on Bayesloc and MicroBayesloc. We thank D. Templeton at the Lawrence Livermore National Laboratory for her kind help in the initial process of this work and for providing access to the Newberry geothermal data set. We also thank the associate editor, L. Eisner, the reviewer, O. Poliannikov, and the two anonymous reviewers for their constructive comments and suggestions.

REFERENCES

Aki, K., and P. Richards, 1980, Quantitative seismology: Theory and methods: WH Freeman & Co.

Artman, B., I. Podladtchikov, and B. Witten, 2010, Source location using time-reverse imaging: Geophysical Prospecting, **58**, 861–873, doi: 10.1111/j.1365-2478.2010.00911.x.

Artman, B., and B. Witten, 2011, Wave-equation microseismic imaging and event selection in the image domain: 81st Annual International Meeting, SEG, Expanded Abstracts, 1699–1703.

Cladouhos, T. T., S. Petty, Y. Nordin, M. Moore, K. Grasso, M. Uddenberg, M. Swyer, B. Julian, and G. Foulger, 2013, Microseismic monitoring of Newberry volcano EGS demonstration: Proceedings of the 38th Workshop on Geothermal Reservoir Engineering, SGP-TR-198.

Douglas, A., 1967, Joint epicentre determination: Nature, **215**, 47–48, doi: 10.1038/215047a0.

Drew, J. E., H. D. Leslie, P. N. Armstrong, and G. Michard, 2005, Automated microseismic event detection and location by continuous spatial mapping: Presented at the SPE Annual Technical Conference and Exhibition, SPE 95513.

Duncan, P. M., and L. Eisner, 2010, Reservoir characterization using surface microseismic monitoring: Geophysics, **75**, no. 5, 75A139–75A146, doi: 10.1190/1.3467760.

Eisner, L., P. M. Duncan, W. M. Heigl, and W. R. Keller, 2009, Uncertainties in passive seismic monitoring: The Leading Edge, **28**, 648–655, doi: 10.1190/1.3148403.

Eisner, L., and J. H. Le Calvez, 2007, New analytical techniques to help improve our understanding of hydraulically induced microseismicity and fracture propagation: Presented at the SPE Annual Technical Conference and Exhibition, doi: 10.2118/110813-MS.

Gesret, A., N. Desassis, M. Noble, T. Romary, and C. Maisons, 2015, Propagation of the velocity model uncertainties to the seismic event location: Geophysical Journal International, **200**, 52–66, doi: 10.1093/gji/ggu374.

Grechka, V., and A. A. Duchkov, 2011, Narrow-angle representations of the phase and group velocities and their applications in anisotropic velocity-model building for microseismic monitoring: Geophysics, **76**, no. 6, WC127–WC142, doi: 10.1190/geo2010-0408.1.

Grechka, V., P. Singh, and I. Das, 2011, Estimation of effective anisotropy simultaneously with locations of microseismic events: Geophysics, **76**, no. 6, WC143–WC155, doi: 10.1190/geo2010-0409.1.

Grechka, V., and S. Yaskevich, 2013, Inversion of microseismic data for triclinic velocity models: Geophysical Prospecting, **61**, 1159–1170, doi: 10.1111/1365-2478.12042.

Hayles, K., R. L. Horine, S. Checkles, and J. Blangy, 2011, Comparison of microseismic results from the Bakken formation processed by three different companies: Integration with surface seismic and pumping data: 81st Annual International Meeting, SEG, Expanded Abstracts, 1468–1472.

Jansky, J., V Plicka, and L. Eisner, 2010, Feasibility of joint 1D velocity model and event location inversion by the neighbourhood algorithm: Geophysical Prospecting, **58**, 229–234, doi: 10.1111/j.1365-2478.2009.00820.x.

Kalman, R. E., 1960, A new approach to linear filtering and prediction problems: Journal of Basic Engineering, **82**, 35–45, doi: 10.1115/1.3662552.

Li, J., C. Li, S. A. Morton, T. Dohmen, K. Katahara, and M. Nafi Toksoz, 2014, Micro-seismic joint location and anisotropic velocity inversion for hydraulic fracturing in a tight Bakken reservoir: Geophysics, **79**, no. 9, C111–C122, doi: 10.1190/geo2013-0345.1.

Li, J., H. Zhang, W. L. Rodi, and M. N. Toksoz, 2013, Joint microseismic location and anisotropic tomography using differential arrival times and differential backazimuths: Geophysical Journal International, **195**, 1917–1931, doi: 10.1093/gji/ggt358.

Li, L., and B. Jafarpour, 2010, Effective solution of nonlinear subsurface flow inverse problems in sparse bases: Inverse Problems, **26**, 105016, doi: 10.1088/0266-5611/26/10/105016.

Matzel, E., D. Templeton, A. Petersson, and M. Goebel, 2014, Imaging the Newberry EGS site using seismic interferometry: Proceedings of the 39th Workshop on Geothermal Reservoir Engineering, SGP-TR-202.

Maxwell, S., 2009, Microseismic location uncertainty: CSEG Recorder, **34**, 41–46.

Maxwell, S., 2014, Microseismic imaging of hydraulic fracturing: Improved engineering of unconventional shale reservoirs: SEG.

Monteiller, V., J.-L. Got, J. Virieux, and P. Okubo, 2005, An efficient algorithm for double difference tomography and location in heterogeneous media, with an application to the Kilauea volcano: Journal of Geophysical Research: Solid Earth, **110**, B12306, doi: 10.1029/2004JB003466.

Myers, S. C., G. Johannesson, and W. Hanley, 2007, A Bayesian hierarchical method for multiple-event seismic location: Geophysical Journal International, **171**, 1049–1063, doi: 10.1111/j.1365-246X.2007.03555.x.

Myers, S. C., G. Johannesson, and W. Hanley, 2009, Incorporation of probabilistic seismic phase labels into a Bayesian multiple-event seismic locator: Geophysical Journal International, **177**, 193–204, doi: 10.1111/j.1365-246X.2008.04070.x.

Oliver, D. S., N. He, and A. C. Reynolds, 1996, Conditioning permeability fields to pressure data: Presented at the ECMOR V-5th European Conference on the Mathematics of Oil Recovery, 259–270.

Oliver, D. S., A. C. Reynolds, and N. Liu, 2008, Inverse theory for petroleum reservoir characterization and history matching: Cambridge University Press.

Osborn, W. L., S. Petty, T. T. Cladouhos, J. Iovenitti, L. Nofziger, O. Callahan, D. S. Perry, and P. L. Stern, 2011, Newberry volcano EGS demonstration-phase I results: Technical report, AltaRock Energy Inc.

Osborn, W., S. Petty, L. Nofziger, and D. Perry, 2010, Newberry volcano EGS demonstration: Geothermal Resources Council Transactions, **34**, 1213–1220.

Petty, S., Y. Nordin, W. Glassley, T. T. Cladouhos, and M. Swyer, 2013, Improving geothermal project economics with multi-zone stimulation: Results from the Newberry volcano EGS demonstration: Proceedings of the 38th Workshop on Geothermal Reservoir Engineering, SGP-TR-19.

Poliannikov, O. V., M. Prange, A. Malcolm, and H. Djikpesse, 2013, A unified Bayesian framework for relative microseismic location: Geophysical Journal International, **194**, 557–571, doi: 10.1093/gji/ggt119.

Poliannikov, O. V., M. Prange, A. E. Malcolm, and H. Djikpesse, 2014, Joint location of microseismic events in the presence of velocity uncertainty: Geophysics, **79**, no. 6, KS51–KS60, doi: 10.1190/geo2013-0390.1.

Rutledge, J. T., and W. S. Phillips, 2003, Hydraulic stimulation of natural fractures as revealed by induced microearthquakes, Carthage Cotton Valley gas field, east Texas: Geophysics, **68**, 441–452, doi: 10.1190/1.1567214.

Slawinski, R. A., and M. A. Slawinski, 1999, On raytracing in constant velocity-gradient media: Calculus approach: Canadian Journal of Exploration Geophysics, **35**, 24–27.

Song, F., and M. N. Toksöz, 2011, Full-waveform based complete moment tensor inversion and source parameter estimation from downhole microseismic data for hydrofracture monitoring: Geophysics, **76**, no. 6, WC103–WC116, doi: 10.1190/geo2011-0027.1.

Tan, Y., C. Chai, and T. Engelder, 2014, Use of S-wave attenuation from perforation shots to map the growth of the stimulated reservoir volume in the Marcellus gas shale: The Leading Edge, **33**, 1090–1096, doi: 10.1190/tle33101090.1.

Tarantola, A., 2005, Inverse problem theory and methods for model parameter estimation: SIAM.

Tarantola, A., and B. Valette, 1982, Inverse problems = quest for information: Journal of Geophysics, **50**, 150–170.

Templeton, D. C., G. Johannesson, and S. C. Myers, 2014, An investigation of the microseismicity at the Newberry EGS site: Technical report, Lawrence Livermore National Laboratory (LLNL).

Waldhauser, F., and W. L. Ellsworth, 2000, A double-difference earthquake location algorithm: Method and application to the northern Hayward Fault, California: Bulletin of the Seismological Society of America, **90**, 1353–1368, doi: 10.1785/0120000006.

Warpinski, N., 2009, Microseismic monitoring: Inside and out: Journal of Petroleum Technology, **61**, 80–85, doi: 10.2118/118537-JPT.

Zhang, H., S. Sarkar, M. N. Toksoz, H. S. Kuleli, and F. Al-Kindy, 2009, Passive seismic tomography using induced seismicity at a petroleum field in Oman: Geophysics, **74**, no. 6, WCB57–WCB69, doi: 10.1190/1.3253059.

Zhang, H., and C. Thurber, 2006, Development and applications of double-difference seismic tomography: Pure and Applied Geophysics, **163**, 373–403, doi: 10.1007/s00024-005-0021-y.

Zhang, H., and C. H. Thurber, 2003, Double-difference tomography: The method and its application to the Hayward fault, California: Bulletin of the Seismological Society of America, **93**, 1875–1889, doi: 10.1785/0120020190.

Zhang, Z., B. Jafarpour, and L. Li, 2014, Inference of permeability heterogeneity from joint inversion of transient flow and temperature data: Water Resources Research, **50**, 4710–4725, doi: 10.1002/2013WR013801.

Zhang, Z., J. W. Rector, and M. J. Nava, 2015a, Microseismic event location using multiple arrivals: Demonstration of uncertainty reduction: Presented at the Unconventional Resources Technology Conference (URTEC).

Zhang, Z., J. W. Rector, and M. J. Nava, 2015b, Improving microseismic event location accuracy with head wave arrival time: Case study using Marcellus shale: 85th Annual International Meeting, SEG, Expanded Abstracts, 2473–2478.

Zhou, R., L. Huang, and J. Rutledge, 2010, Microseismic event location for monitoring CO_2 injection using double-difference tomography: The Leading Edge, **29**, 208–214, doi: 10.1190/1.3304826.